BMC Cancer

RESEARCH Open Access

Characterisation of a novel p53 mutation ($p53_{N263Tfs*7}$) associated with li-fraumeni syndrome

Francesca M. Wright[1], Mariela Vasileva-Slaveva[2,3], Angel Yordanov[4], Ivan Ivanov[4], Zornitsa Gorcheva[4], Andrea Mohr[1], Gareth S. A. Wright[1], Greg N. Brooke[1*] and Metodi V. Metodiev[1,4*]

Abstract

Li-Fraumeni Syndrome (LFS) is a hereditary cancer predisposition syndrome caused by germline mutations in the *TP53* tumour suppressor gene, which encodes the multifunctional transcription factor p53. p53 is the most commonly mutated protein in human cancer, with the majority occurring within the DNA-binding domain, often disrupting transcriptional activity and resulting in a loss-of-function. Here, we characterise the novel $p53_{N263Tfs*7}$ truncated mutant, identified as a germline mutation from a patient with LFS who developed breast cancer. Functional assays revealed a partial loss-of-function across key cellular processes, including proliferation, cell death, cell motility, and transcriptional transactivation. This mutant lacked a dominant-negative effect, distinguishing it from common DNA-binding domain missense mutations. Our findings demonstrate that oncogenesis in LFS can be driven by partial impairment of functional p53, rather than dominant-negative or gain-of-function mutations alone. This underscores the clinical significance of recognising subtle *TP53* variants for the refined molecular classification and clinical prediction of cancer risk in *TP53* mutation carriers.

Keywords TP53 , Lee-Fraumeni Syndrome, Mutations, Breast cancer

Background

In 1969, Frederick Li and Joseph Fraumeni described four families in which multiple children had developed soft-tissue sarcomas, with early-onset cancers also observed in at least one young adult within the family [1]. As a result, they suggested a hereditary syndrome of cancer predisposition [2], which is now known as Li-Fraumeni Syndrome (LFS). It is now understood that the majority of families (∼ 70–80%) meeting the classic LFS criteria carry a pathogenic germline *TP53* mutation [3–5]. *TP53* is a tumour suppressor gene that plays a pivotal role in maintaining genomic integrity and cellular homeostasis [6]. Its encoded protein, p53, is regulated by post-translational modifications, such as phosphorylation, acetylation, and ubiquitination [7]. Stabilising post-translational modifications generally occur in response to various cellular stresses, including DNA damage, hypoxia, and oncogene activation [8]. This stabilisation and activation of p53 allows it to carry out functions in a variety of different processes, including DNA repair mechanisms, programmed cell death pathways (such as apoptosis and autophagy) [9], and the induction of cell cycle arrest and cellular senescence [7].

*Correspondence:
Greg N. Brooke
gbrooke@essex.ac.uk
Metodi V. Metodiev
mmetod@essex.ac.uk
[1]School of Life Sciences, University of Essex, Colchester, Essex CO4 3SQ, UK
[2]Department of Breast Surgery, Shterev Hospital, Sofia 1000, Bulgaria
[3]Bulgarian Breast and other gynecological Cancers Association, Sofia 1750, Bulgaria
[4]Medical University of Pleven, Pleven 5800, Bulgaria

© The Author(s) 2026. **Open Access** This article is licensed under a Creative Commons Attribution 4.0 International License, which permits use, sharing, adaptation, distribution and reproduction in any medium or format, as long as you give appropriate credit to the original author(s) and the source, provide a link to the Creative Commons licence, and indicate if changes were made. The images or other third party material in this article are included in the article's Creative Commons licence, unless indicated otherwise in a credit line to the material. If material is not included in the article's Creative Commons licence and your intended use is not permitted by statutory regulation or exceeds the permitted use, you will need to obtain permission directly from the copyright holder. To view a copy of this licence, visit http://creativecommons.org/licenses/by/4.0/.

TP53 is the most frequently mutated gene in human cancers [10, 11], with the majority occurring within the DNA-binding domain (DBD) [12]. This pattern is replicated in LFS-associated *TP53* mutations, as missense mutations in the DBD comprise the vast majority of germline *TP53* mutations [3]. As a consequence of mutations, p53's binding to downstream response elements (REs) is compromised, often leading to loss-of-function (LOF) [13]. Further to this observed LOF, gain-of-function mutations (GOF), which confer oncogenic activity onto the mutant p53 protein, have also been suggested [14]. This aspect of p53 mutations is a controversial topic, and a wealth of literature exists both accepting and refuting claims of GOF p53 mutations [12].

The dominant-negative activity of specific p53 mutations is a well-recognised mechanism of tumour suppression loss [15]. Given that the majority of p53 mutations are found within the DBD, mutants often retain the capacity to oligomerise, forming functional tetrameric complexes, and it has subsequently been demonstrated that wild-type and mutant p53 proteins can form inhibitory heterotetramer complexes [16]. In instances where dominant-negative effects (DNE) are active, mutant subunits within the heterotetramer may induce conformational changes in wild-type subunits and function is subsequently abrogated [15]. Further, the extent of the DNE appears to correlate with the number of mutant p53 subunits in the heterotetramer complex [17]. DNEs often play a critical role in the oncogenesis of p53 heterozygous tumours, due to the ability to attenuate the tumour-suppressing functions of wild-type p53 through heterotetramer complex formation [12].

Importantly, not all *TP53* mutations are expected to behave equivalently. While the majority of cancer-associated and LFS-associated *TP53* variants are missense mutations within the DBD that retain an intact tetramerisation domain, a smaller subset consists of truncating variants that result in loss of all or part of the C-terminus. Studies have demonstrated substantial heterogeneity among *TP53* variants, with missense mutants frequently exhibiting dominant-negative activity and, in some cases, GOF properties, whereas truncating variants are generally associated with loss of protein function and reduced capacity to interfere with wild-type p53 [18, 19]. Consequently, the functional consequences of *TP53* truncating mutations cannot be inferred solely from studies of common DNA-binding domain missense mutants.

Despite its low prevalence, LFS is highly penetrant, such that carriers of germline *TP53* mutations have a 50% probability of developing cancer by age 30 [20], increasing to a 90% probability within the lifetime of the carrier [21]. This compares to germline *BRCA1/BRCA2* mutations, which are significantly more common among the general population, but carry a lower risk of breast cancer development than germline *TP53* mutations [22]. Furthermore, it has been shown that penetrance is highly dependent on both the cancer tissue type and the gender of the carrier [23].

In this study, a novel p53 mutation identified from a patient diagnosed with LFS, and a paternal history of cancer was characterised. This patient presented with osteosarcoma of the knee at an early age and subsequently developed breast cancer at 27. The mutation in question consists of a 5 bp deletion in exon 8 (NM_000546.6:c.788_792del), resulting in a frameshift and the introduction of a premature stop codon 7 amino acids downstream, at position 269. This truncated protein (NP_000537.3:p.(N263Tfs*7)), now referred to as N263Tfs*7, lacks the C-terminus, which houses the tetramerisation domain (TD). To elucidate the functional consequences of this truncation, we performed a series of experiments; comparing our mutant to both wild-type p53 and a transcriptionally inactive control mutant, C135Y [24]. Overall, our findings indicate that the N263Tfs*7 mutation is hypomorphic, resulting in severely compromised tumour suppressive activity across proliferation, cell death, motility, and transcriptional transactivation. By characterising $p53_{N263Tfs*7}$, we demonstrate that a partial, quantitative reduction in functional p53 levels can be sufficient to drive oncogenesis in the context of LFS, highlighting the need for a more nuanced molecular classification of *TP53* variants, as recognising these subtle impairments may support more accurate clinical risk prediction and management in mutation carriers.

Methods

3D modelling of $p53_{N263Tfs*7}$

Protein domain maps were prepared for $p53_{WT}$, $p53_{C135Y}$, and $p53_{N263Tfs*7}$ using the drawProteins package [25] in R v4.3.2 [26]. Invasive breast carcinoma datasets from cBioPortal [27–29], were compiled and used to identify p53 mutations. The amino acid sequence for $p53_{N263Tfs*7}$ was used to predict the 3-dimensional structure of the mutant protein using AlphaFold3 [30]. The predicted structure, and the 4HJE wild-type tetrameric crystal structure of the p53 core domain in the presence of DNA [31] were compared using PyMol v3.1.6.1 [32].

Site-directed mutagenesis

GFP-tagged $p53_{WT}$ was synthesised and cloned into a pTWIST expression vector (pTWIST-GFP-$p53_{WT}$). Mutagenesis primers for $p53_{C135Y}$ and $p53_{N263Tfs*7}$ were designed using the Agilent QuikChange Primer Design tool, and ordered from IDT (Table 1). Mutagenesis was performed using an Agilent QuikChange II Site-Directed Mutagenesis Kit according to the manufacturer's instructions, with the following modification: 2.9% (v/v) DMSO

was also added to each mutagenesis reaction. Successful mutagenesis was confirmed using Sanger sequencing.

Cell culture

Cells were acquired from ATCC, and frozen at a low passage. Cells were cultured in Dulbecco's Modified Eagle's Medium, supplemented with 10% (v/v) Fetal Bovine Serum. Cells were passaged twice weekly. Fresh aliquots were defrosted every six months.

Western blotting

HeLa cells were grown to 70–90% confluency in a 6-well plate and transfected with 4 μg of pTWIST-GFP constructs using TurboFect, following the manufacturer's instructions. Cells were harvested using a cell scraper and pelleted (1,500 rpm for 3 min). The supernatant was aspirated and the cells washed with 1 ml PBS. Cells were re-pelleted (1,500 rpm for 3 min), the supernatant aspirated, and the pellet lysed in RIPA buffer. Western blotting was performed as described [33], with the following modifications: 40 μg of protein was separated, and electrophoretic transfer onto nitrocellulose membranes was performed using the iBlot™ 2 Gel Transfer Device. Primary antibodies used were; GFP B-2 (Santa Cruz Biotechnology, sc-9996), p53 (Dako, M3629), and α-tubulin (Proteintech, 11224-1-AP). HRP-conjugated secondary antibodies used were; anti-mouse (Proteintech, SA00001-1), and anti-rabbit (Proteintech, SA00001-2). Densitometry quantifications were performed using ImageJ 1.54g [34].

Fluorescence imaging

HeLa cells were seeded onto glass coverslips at a seeding density of 5×10^5 cells/ml in a 12-well plate. Cells were transfected with 2 μg of pTWIST-GFP constructs using TurboFect, following the manufacturer's instructions, and incubated for 24 h. Cells were fixed in 2% w/v PFA at room temperature for 10 min, washed with PBS and mounted on slides using DAPI mountant (ProLong™ Gold Antifade Mountant, Invitrogen). Images were acquired using an EVOS M5000 Imaging System. Image analysis was performed using ImageJ [34], to separate and quantify the nuclear and cytoplasmic GFP signals.

Subcellular protein fractionation

HEK293S cells were grown to 70–90% confluency in a 6-well plate and transfected with 4 μg of plasmid using TurboFect. Subcellular protein fractionation was performed using a Subcellular Protein Fractionation Kit for Cultured Cells (Thermo Scientific), following the manufacturer's instructions. Protein localisation was visualised by Western blotting and probing with anti-GFP antibody (Santa Cruz Biotechnology, sc-9996), as described (Western blotting).

Luciferase reporter assay

HeLa cells were grown to 70–90% confluency in a 24-well plate and transfected with 200 ng pTWIST-GFP constructs, 200 ng p21luc plasmid, and 100 ng BOS-β-Gal plasmid using a calcium phosphate transfection method [35]. 24 h after transfection, cells were washed with PBS and fresh media added. Cells were incubated for a further 24 h before lysis and subsequent luciferase and β-galactosidase activities were measured, as described [36]. Luciferase activity was normalised to β-galactosidase activity, and expressed as a percentage of pTWIST-GFP-p53$_{WT}$ activity.

Quantitative PCR analysis of gene expression

HeLa cells were seeded in 12 well plates, transfected with 1 μg of pTWIST-GFP-p53 construct using Turbofect and incubated for 48 h prior to collection. RNA extraction and qPCR was performed as previously described [37] and gene expression normalised to transfection efficiency (% GFP positive cells). Primer sequences (5'–3'): *L19* F – GCGGA AGGGTACAGCCAAT, *L19* R – GCAGCCGGCGCAAA; *p21* F – GACACCACTGGAGGGTGACT; *p21* R – CAGG TCCACATGGTCTTCCT; *BAX* F – CCCGAGAGGTCCT TTTCCG, BAX R – GCACTCCCGCCACAAAGAT.

Caspase-GLO 3/7 assay

HEK293T cells were grown to 70–90% confluency in a 6-well plate and transfected with 4 μg pTWIST-GFP constructs using TurboFect. Transfected cells were sub-cultured into 96-well plates at a seeding density of 3.6×10^4 cells/ml. Cells were incubated for 72 hours before imaging using a SARTORIOUS Incucyte S3 to quantify the number of GFP-positive cells. Caspase-GLO 3/7 assay was performed according to the manufacturer's instructions. The luminescence for each pTWIST-GFP construct was normalised to the corresponding number of GFP-positive cells and expressed as a percentage of caspase-3/7 activity in pTWIST-GFP (Empty) control.

Growth assay

HEK293T cells were grown to 70–90% confluency in a 6-well plate and transfected with 4 μg pTWIST-GFP constructs using TurboFect. Transfected cells were sub-cultured into a 24-well plate at a seeding density of 6×10^4 cells/ml. Images were acquired in six-hour intervals, using a SARTORIUS Incucyte S3, for three days.

Wound healing assay

HEK293T cells were grown to 70–90% confluency in a 6-well plate and transfected with 4 μg pTWIST-GFP constructs using TurboFect. Using a P10 micropipette tip, "wounds" were scratched into the bottom of each transfected well. Media was aspirated, cells were washed with PBS, and fresh media added. Images were acquired in four-hour intervals, using a SARTORIUS Incucyte S3,

for two days. Images were exported and the area of the scratch analysed in ImageJ [34], using Manual Wound Healing Size Tool for stack analysis [38].

CRISPR-select^{TIME} assay

HEK293T cells were grown to 70–90% confluency in a 24-well plate. 1 μg of donor DNA (the $p53_{N263Tfs*7}$ mutant or a synonymous WT control, $p53_{SYN}$, used for internal normalisation; Table 2) was transfected into cells using Lipofectamine CRISPRMAX Reagent (Thermo Scientific) RNP method, with 1 μg purified Cas9 protein and 250 ng gRNA (Table 2). Donor DNA and gRNA were designed using Invitrogen TrueDesign Genome Editor [39]. For mixing of cell populations, cells were trypsinised, resuspended in media and centrifuged (2000 rpm, 4 min). The pellets were resuspended in media, the cell suspensions combined, and split equally into a 24-well plate. For each condition, two independent CRISPR editing/transfection experiments were performed. Following transfection, cells from the two independent experiments were combined and seeded as a single mixed cell population for subsequent harvesting and analysis.

For harvesting of mixed cell populations, cells were trypsinised, resuspended in media and centrifuged (2000 rpm, 4 min). The pellets were frozen at −70 °C until further processing. Cells were harvested in 24-hour intervals. Genomic DNA was isolated using 0.2 M NaOH and regions of interest were amplified using PCR amplification (Table 2); Q5 High-Fidelity DNA Polymerase (New England BioLabs). Products were separated using agarose gel electrophoresis, and purified using a GeneJET Gel Extraction and DNA Cleanup Micro Kit (Thermo Scientific). The DNA concentration was measured using a NanoDrop spectrophotometer, and samples sent to GENEWIZ UK Ltd for NGS. FASTQ files were subsequently analysed using MutScan v1.14.1 [40], by defining the left flanking sequence, the specified mutation, and the right flanking sequence for each CRISPR-induced mutation (Table 3).

Statistical analyses

For the fluorescence microscopy image analysis and qPCR, one-way ANOVA and post-hoc (Tukey's HSD) tests were performed using R v4.3.2 [26]. For the luciferase reporter and Caspase-GLO 3/7 assays one-tailed heteroscedastic t-tests were performed. For the growth and wound healing assays, ANOVA and post-hoc (Tukey's HSD) tests were performed using R v4.3.2 [26], and Bonferroni correction was applied.

Results

$p53_{N263Tfs*7}$ leads to a premature stop codon in the DNA binding domain

A novel p53 mutation was identified in a patient with LFS. The patient was originally diagnosed with sarcoma and then developed breast cancer. Sequencing analysis of the individual's blood sample identified a heterozygous germline p53 mutation that consisted of a deletion of ATCTA starting at Asn263. The resulting frameshift introduces six new amino acids (Thr-Gly-Thr-Glu-Gln-Leu) before a premature stop codon at position 269. The truncated protein subsequently lacks the 3' end of the DBD, the TD, and the C-terminal regulatory domain, as well as the nuclear localisation signal (NLS) and the nuclear export signal (NES). To better understand if this region of p53 is commonly mutated in breast cancer, the cBioPortal repository was interrogated [27–29]. Missense mutations in the DBD were the most frequently observed alteration, while 15% of the patient samples analysed exhibited truncations (Fig. 1a). The asparagine residue at position 263 is rarely mutated in breast cancer, occurring in 0.08% of the analysed patient samples.

To investigate the potential effect of the truncation upon p53, AlphaFold3 was used to predict the 3-dimensional structure of $p53_{N263Tfs*7}$, and the resulting structure was overlaid with the 4HJE crystal structure of the $p53_{WT}$ core domain (Fig. 1b). The $p53_{N263Tfs*7}$ predicted structure aligns well with $p53_{WT}$, with ordered regions exhibiting greater consensus than disordered regions, with the α -helix at residues 273–291 completely lost. This suggests that DNA binding may be reduced as a result of the truncation, regardless of consensus between the 4HJE crystal structure of the $p53_{WT}$ core domain and the AlphaFold3 predicted structure of $p53_{N263Tfs*7}$.

$p53_{N263Tfs*7}$ results in protein truncation

To generate N-terminally GFP-tagged p53-mutant constructs, site-directed mutagenesis was performed on pTWIST-GFP-$p53_{WT}$ and successful mutagenesis confirmed using Sanger sequencing (Supplementary Table 8). To confirm expression of wild-type and mutant p53, HeLa cells were transfected with N-terminally GFP-tagged p53 constructs and immunoblotting was performed (Fig. 2). As expected, $p53_{WT}$ and $p53_{C135Y}$ were approximately 90 kDa in size (p53 + ∼27 kDa GFP). The truncation caused by $p53_{N263Tfs*7}$ should result in a protein of approximately 36 kDa, which with the GFP-tag should give a fusion protein of 63 kDa, in agreement with what was observed on the western blot. Relative $p53_{C135Y/N263Tfs*7}$ expression was 28.4- and 28.7-fold higher than $p53_{WT}$, respectively, suggesting that these mutants are resistant to the proteasomal degradation which regulates $p53_{WT}$ abundance [41].

$p53_{N263Tfs*7}$ has altered cellular localisation compared to $p53_{WT}$

To analyse the localisation of $p53_{N263Tfs*7}$, HeLa cells were transfected with GFP-tagged constructs and imaged using fluorescent microscopy. pTWIST-GFP was

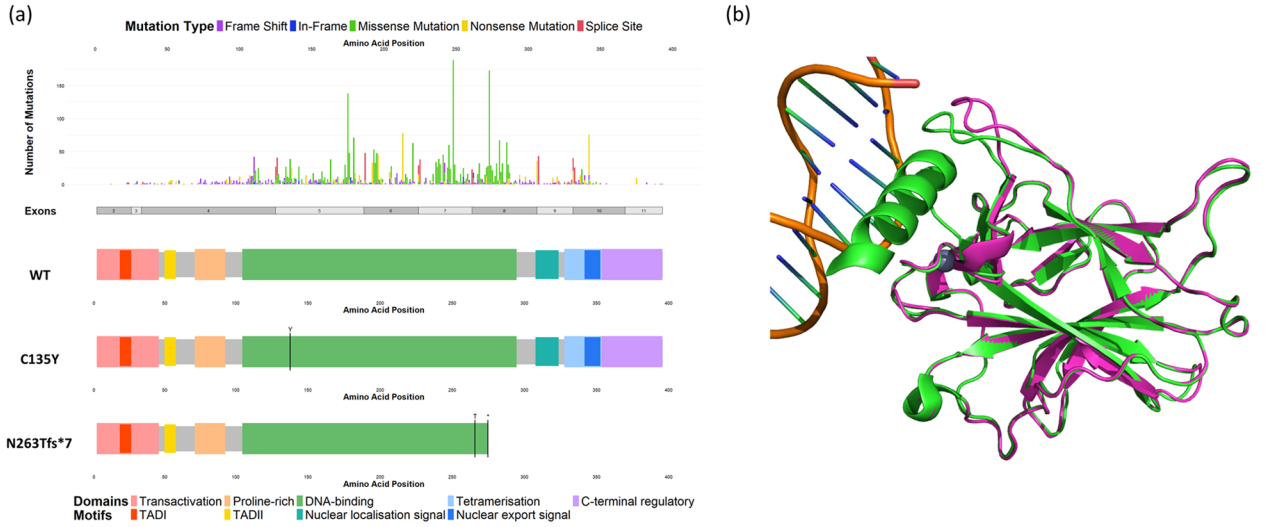


Fig. 1 Analysis of p53 mutations in breast cancer and the structure of $p53_{N263Tfs*7}$. **a** Analysis of p53 mutations by amino acid residue in breast invasive carcinoma was performed, and mapped to exons and domains of p53. The location of the $p53_{C135Y}$ point mutation and $p53_{N263Tfs*7}$ deletion start site are marked with solid black lines and the new amino acids indicated, while the $p53_{N263Tfs*7}$ premature stop codon is marked with a dashed black line. **b** 3-dimensional predictive modelling of $p53_{N263Tfs*7}$ was performed using AlphaFold3 (magenta) and compared to the 4HJE crystal structure of $p53_{WT}$ (green) using PyMol

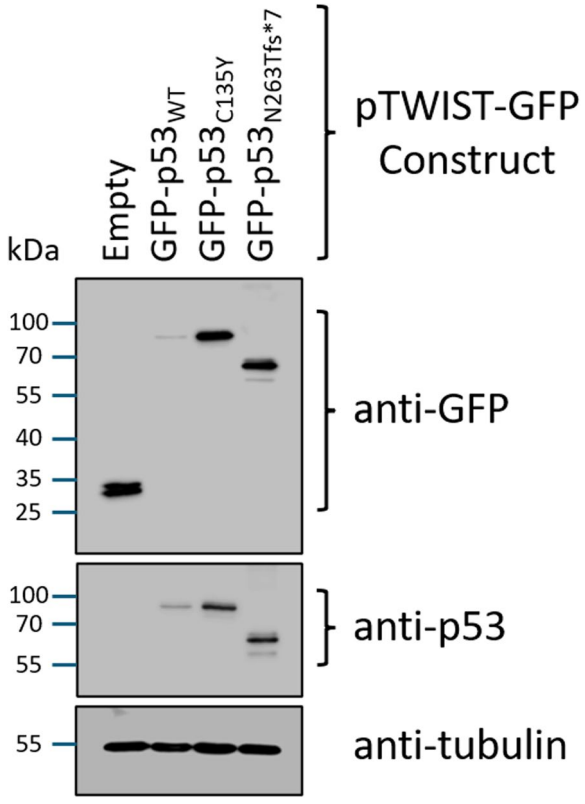


Fig. 2 The $p53_{N263Tfs*7}$ mutation increases protein abundance in HeLa cells. HeLa cells were grown and transfected with N-terminally GFP-tagged p53 constructs. Equal amounts of protein from each transfected culture were subjected to western blot analysis using anti-GFP and anti-p53. Tubulin was used as a loading control. Representative of two independent repeats

observed to localise diffusely throughout the cell, $p53_{WT}$ appeared to predominantly localise to the nuclear compartment (63.9%), while $p53_{C135Y/N263Tfs*7}$ were observed to predominantly localise to the cytoplasmic compartment (31.0% and 36.5% respectively) (Fig. 3a, b). To further analyse the subcellular localisation of p53, cell fractionation was performed. $p53_{WT}$ was found to be predominantly nuclear and chromatin-bound. A significant fraction was also found to be associated with the cytoskeleton. In agreement with the imaging results, $p53_{C135Y}$ was less nuclear than $p53_{WT}$. $p53_{N263Tfs*7}$ had a similar distribution to $p53_{C135Y}$, although there was a significant portion associated with the cytoskeleton (Fig. 3c). Both mutants therefore have reduced nuclear localisation and reduced chromatin binding.

$p53_{N263Tfs*7}$ has reduced transcriptional activity

To analyse the transcriptional activity of $p53_{N263Tfs*7}$, HeLa cells were co-transfected with the GFP-tagged constructs, p21luc and BOS-β-gal plasmids, and luciferase reporter assays performed (Fig. 4a). $p53_{WT}$ increased reporter activity 51-fold compared to basal levels. $p53_{C135Y}$ was found to be transcriptionally inactive, whereas $p53_{N263Tfs*7}$ retained a small amount of transcriptional activity, increasing reporter activity 1.7-fold. As mentioned previously, some p53 mutants appear to have dominant-negative activity over $p53_{WT}$. To determine if $p53_{N263Tfs*7}$ is able to exert dominant-negative or wild-type rescue effects, reporter assays were repeated, with cells co-transfected with pTWIST-GFP-$p53_{WT}$ ± -GFP-$p53_{C135Y/N263Tfs*7}$ (Fig. 4b). Co-transfection with the mutant constructs (at a 1:1:1 molar ratio,

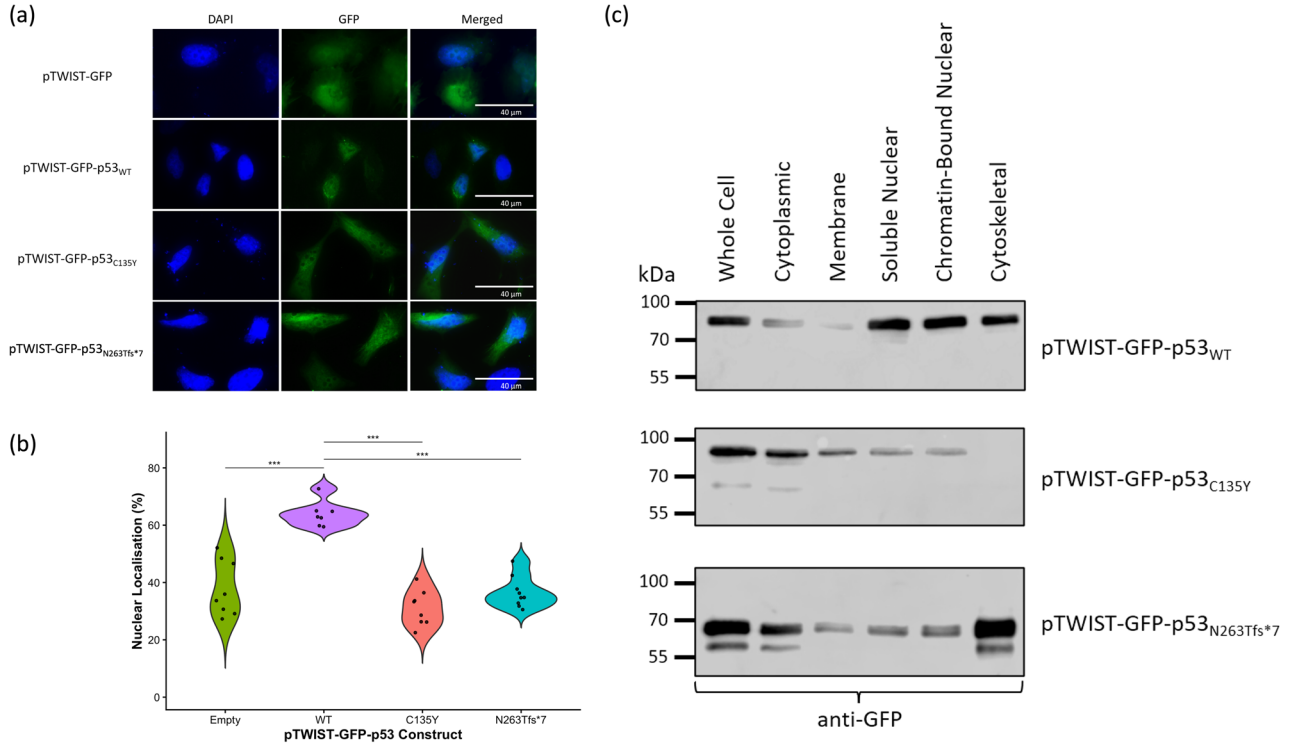


Fig. 3 The $p53_{N263Tfs*7}$ mutation reduces nuclear localisation of the protein. **a** HeLa cells grown on coverslips were transfected with pTWIST-GFP constructs. The subcellular localisation of p53 was determined by staining cells with DAPI mountant and fluorescence imaging, and **b** the nuclear localisation was quantified using ImageJ. *** $p < 0.001$. Localisation analysis was performed on a minimum of 7 cells per construct. **c** HEK293S cells were grown and transfected with pTWIST-GFP-p53 constructs. Proteins from all fractions were subjected to western blotting using anti-GFP antibody. Representative images from 2 independent experiments

$p53_{WT}$:$p53_{N263Tfs*7}$:p21luc) had no significant effect on $p53_{WT}$ activity. Neither of the mutants were therefore found to exert DNE over $p53_{WT}$.

To investigate the effect of the mutants on endogenous gene expression, the levels of the established p53 target genes *p21* and *BAX* were quantified. HeLa cells were transfected with the p53 plasmids or empty control and incubated for 48 h prior to harvesting for qPCR analysis (Fig. 4c). As expected, $p53_{WT}$ significantly increased the expression of both target genes. In contrast, neither mutant altered target gene expression. Although $p53_{N263Tfs*7}$ appeared to increase *BAX* expression (approximately 1.5-fold), this did not reach significance.

$p53_{N263Tfs*7}$ has reduced inhibitory activity upon cell proliferation

To assess the effect of p53 mutants on proliferation, growth assays were performed. HEK293T cells were transfected with GFP-tagged p53 constructs and images were taken every six hours for a total of 72 hours (Fig. 5a). Cells expressing $p53_{C135Y}$ remained in the exponential growth phase longer than cells expressing $p53_{WT/N263Tfs*7}$, with growth beginning to plateau at ~60 hours. Conversely, cells expressing $p53_{WT}$ plateaued considerably earlier, at ~30 hours, while cells expressing $p53_{N263Tfs*7}$ plateaued at an intermediate time point. The $p53_{N263Tfs*7}$ mutation therefore has reduced tumour suppressive activity compared to $p53_{WT}$.

To investigate the effect of $p53_{N263Tfs*7}$ upon proliferation further, HEK293T cells were subjected to CRISPR-Select^{TIME} assays [42]. Mixed cell populations, containing $p53_{N263Tfs*7}$ edited cells and cells containing the WT-synonymous mutation ($p53_{SYN}$), were harvested at 24-hour intervals. The region surrounding the edited bases (~500 bp) was PCR amplified, and the resulting DNA sent for NGS. FASTQ files were analysed using MutScan [40], to determine the relative number of mutant reads over time. The ratio of $p53_{N263Tfs*7}$ edited cells to $p53_{SYN}$ edited cells increased 2.1-fold over the duration of the assay (Fig. 5b). The CRISPR-Select^{TIME} assay data are therefore consistent with a selective advantage of $p53_{N263Tfs*7}$ relative to the $p53_{SYN}$ control, providing supporting evidence that the p53 variant confers proliferative advantages over $p53_{WT}$.

The $p53_{N263Tfs*7}$ truncation impairs pro-apoptotic signalling

As N263Tfs*7 reduced the inhibitory effects of p53 upon proliferation and motility, we were interested to see if this truncation also has an impact upon cell death. To

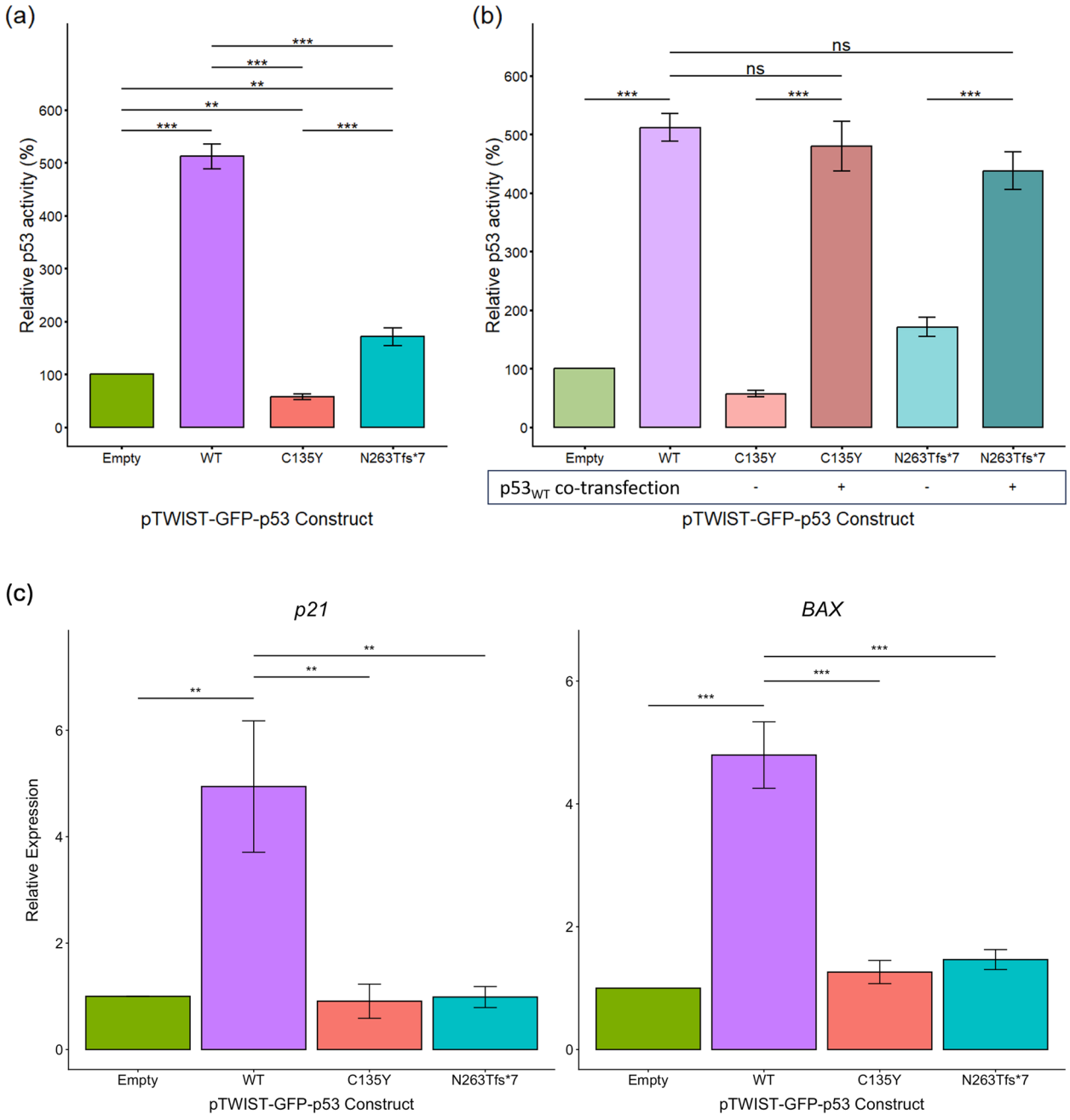


Fig. 4 The $p53_{N263Tfs*7}$ mutation reduces transcriptional transactivation of p53 REs. HeLa cells were grown and co-transfected with p21luc and BOS-β-gal plasmids and **a** 200 ng of pTWIST-GFP constructs or **b** plasmid DNA totalling 400 ng consisting of combinations of either pTWIST-GFP or pTWIST-GFP-$p53_{WT}$, with pTWIST-GFP-$p53_{C135Y/N263Tfs*7}$ constructs. Cells were lysed and subjected to luciferase reporter assays to measure reporter activation and infer activity of p53 mutants. Mean of three independent repeats with duplicates ± SE. t-test ** $p < 0.01$, *** $p < 0.001$, ns = not significant. **c** HeLa cells were grown and transfected with pTWIST-GFP constructs. RNA extraction and qPCR were performed to assess relative expression of *p21* and *BAX* mRNA. Mean of four independent repeats ± SE. ANOVA and Tukey's HSD ** $p < 0.01$, *** < 0.0001

analyse the apoptotic caspase activity of p53 mutants, HEK293T cells were transfected with pTWIST-GFP-p53 constructs and Caspase-3/7 assays performed. $p53_{WT}$ increased caspase 3/7 activity 5.3-fold compared to basal levels. Conversely, $p53_{C135Y}$ resulted in a non-significant 1.3-fold increase. Interestingly, $p53_{N263Tfs*7}$ increased caspase 3/7 activity 3.3-fold, and this was found to be significantly lower than $p53_{WT}$ (Fig. 6). $p53_{N263Tfs*7}$ therefore has reduced pro-apoptotic activity compared to $p53_{WT}$, although some activity is retained.

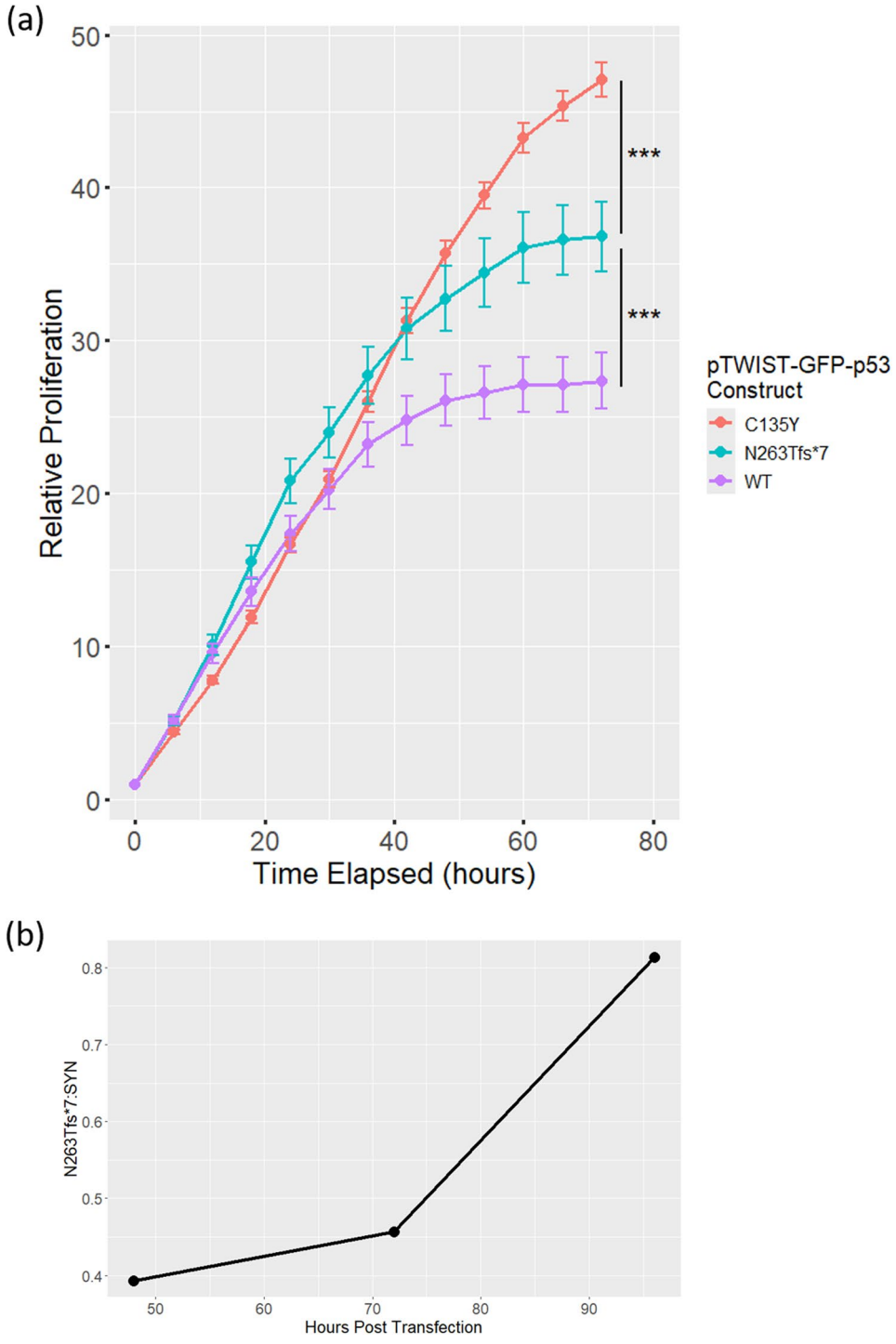


Fig. 5 The $p53_{N263Tfs*7}$ mutation has reduced inhibitory effect upon proliferation. **a** HEK293T cells were grown and transfected with pTWIST-GFP-p53 constructs, and seeded at a low density into a 24-well plate. The total number of green cells were counted and made relative to timepoint 0. A two-way ANOVA was performed, followed by post-hoc testing with Bonferroni correction. Mean of 3 independent repeats, with 6 wells per condition and 4 images taken per well ± SE. ANOVA and Tukey's HSD *** < 0.0001. **b** HEK293T cells were subjected to CRISPR-Select^{TIME} assays. For each condition, two independent CRISPR editing/transfection experiments were performed and pooled prior to initiation of the time course. Amplicon NGS was performed on samples collected at 24 h intervals, and the ratio of $p53_{N263Tfs*7}$ to WT-synonymous mutation ($p53_{SYN}$) reads calculated

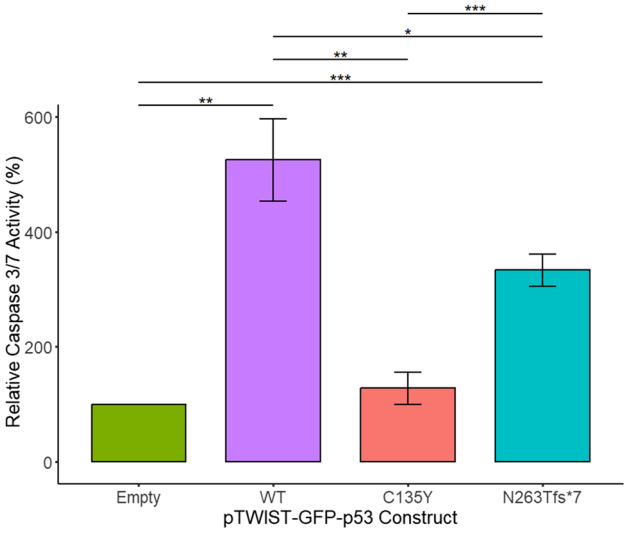


Fig. 6 The $p53_{N263Tfs*7}$ mutation reduces caspase 3/7 apoptotic activity. HEK293T cells were grown and transfected with pTWIST-GFP constructs, and grown in a 24-well plate. Cells were mixed with Caspase-GLO 3/7 reagent, and the luminescent signal measured to show the relative apoptosis induction of p53 mutants. Mean of three independent repeats with duplicates ± SE. t-test * $p < 0.05$** $p < 0.01$, *** $p < 0.001$

The $p53_{N263Tfs*7}$ mutation inhibits anti-metastatic tumour suppressive functions

p53 mutants are typically associated with invasive and metastatic cancers, suggesting a role for p53 in cell migration [43]. To assess the effect of p53 mutants on migration, HEK293T cells were transfected with the p53 constructs. "Wounds" were introduced into the cell monolayer, and images taken every 4 hours (Fig. 7a). After 48 hours, both pTWIST-GFP and $p53_{C135Y}$ exhibited almost complete wound closure, while $p53_{WT}$ showed very low levels of wound closure. $p53_{N263Tfs*7}$ showed intermediate levels of wound closure, significantly different from $p53_{WT/C135Y}$ (Fig. 7b). Over the 48-hour period, $p53_{WT}$ and $p53_{N263Tfs*7}$ also showed a decrease in monolayer density (Fig. 7a). As with previous experiments, $p53_{N263Tfs*7}$ therefore has reduced, but not completely impaired, tumour suppressor activity.

Discussion

This study investigated the functional implications of a novel germline p53 mutation identified in a blood sample from a breast cancer patient diagnosed with LFS and a previous osteosarcoma diagnosis. p53 is a well-studied protein, with considerable literature dissecting its involvement in several key mechanisms and pathways. Our aim was to determine the functional consequences associated with this novel mutation, and we subsequently demonstrated that $p53_{N263Tfs*7}$ is a hypomorphic LOF mutant that retains residual transcriptional and tumour-suppressive activity, distinctly lacking DNE upon $p53_{WT}$.

Mutations in the DBD of p53 are well-documented, representing the most common alteration in p53 [44]. Analysis of cBioPortal breast invasive carcinoma datasets [27–29], found that mutations at residue 263 are rare, accounting for ∼0.08% of mutations. This translates to only three reported mutations in this location, all of which were frame shift mutations. The frame shift associated with $p53_{N263Tfs*7}$ results in the introduction of a stop codon at position 269.

To assess the potential structural basis for observed functional defects, the 3D conformation of $p53_{N263Tfs*7}$ was predicted and compared to the crystal structure of wild-type p53 in the presence of DNA [31]. The model did not show significant conformational deviations from the wild-type structure, despite lacking the H2 α-helix at residues 278–292 [45]. The H2 helix sits in the DNA major groove [46], allowing A276, C277 and R280 to form hydrogen bonds and hydrophobic interactions at the major groove [47]. The R273 residue, which is also deleted in the $p53_{N263Tfs*7}$ mutant, is also critical for DNA binding at the major groove, due to a direct interaction with the DNA backbone [47]. Mutations at R273 are common in cancer, with the residue classed as a "hotspot" for cancer-associated mutations [48], which are known to abrogate DNA binding [49]. Therefore, the $p53_{N263Tfs*7}$ deletion leaves fewer of the critical DNA-binding residues intact, suggesting that interaction with DNA will be significantly attenuated, consistent with the tempered transcriptional activity observed in the reporter assays.

p53's tumour suppressor functions are critically dependent on its activation via post-translational modifications and subsequent nuclear translocation [50]. However, many p53 mutants exhibit altered subcellular localisation patterns, with notable aberrant cytoplasmic sequestration observed in various tumour types [51]. This phenomenon is often correlated with poor prognosis, and poor responses to chemotherapy [52, 53], prompting investigations into its underlying mechanisms. In the context of our study, localisation experiments revealed that a large proportion of $p53_{N263Tfs*7}$ was extranuclear. Specifically, we observed that $p53_{N263Tfs*7}$ exhibited a predominantly cytoplasmic distribution, accompanied by a noticeable reduction in nuclear (both soluble and chromatin-bound) accumulation compared to $p53_{WT}$. This finding aligns with previous reports of cytoplasmic sequestration for other p53 mutants. The cytoplasmic retention of mutant p53, as observed for N263Tfs*7, could stem from several factors. Given that N263Tfs*7 involves a truncation that excludes residues 269–393, encompassing the 3' end of the DBD, the TD, and the C-terminal domain, including the NLSs and NES [54]. It is therefore likely that the altered localisation is due to the lack of the NLSs [55], with conformational changes, the presumed inability to tetramerise [56], and a possible

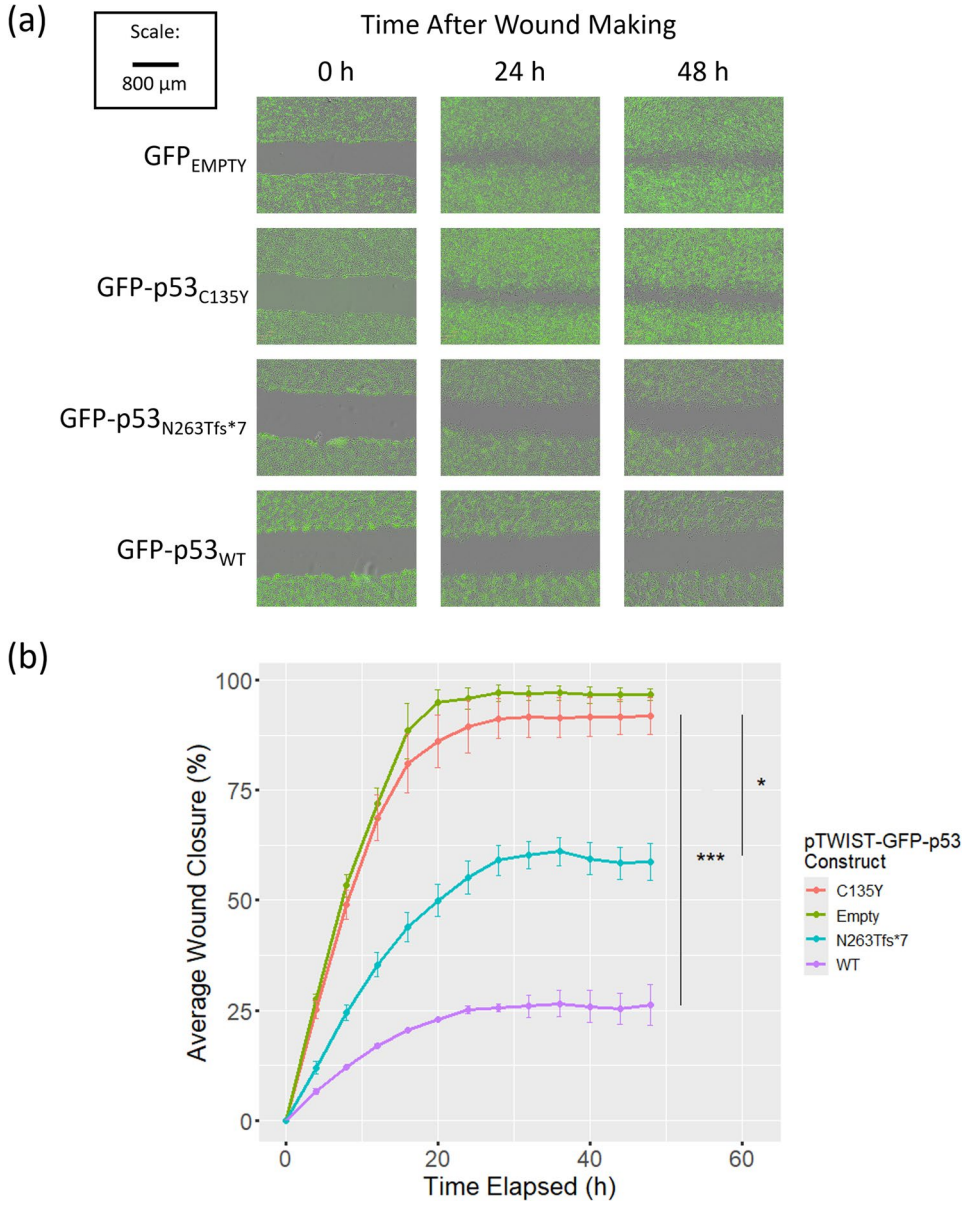


Fig. 7 The p53$_{N263Tfs*7}$ mutation increases the migratory capacity of cells in culture. HEK293T cells were grown and transfected with pTWSIT-GFP constructs, and wounds scratched into the bottom of each well. (A) Images were acquired every 4 hours using SARTORIUS Incucyte S3, and (B) the area of the wound at each time point was analysed using Manual Wound Healing Size Tool for stack analysis in ImageJ. One-way ANOVA and Tukey's HSD analyses were performed, with Bonferroni correction. Mean of 3 independent repeats, with 3 images taken per well ± SE. ANOVA and Tukey's HSD * $p < 0.05$, *** $p < 0.0001$

increased affinity for cytoskeletal filament systems [57], contributing to its cytoplasmic sequestration.

While p53 predominantly exerts tumour suppressive functions through its role as a transcription factor, mislocalisation to the cytoplasm is significant as p53 has also been shown to play a role in cytoplasmic functions, including mitochondrial-driven apoptosis [58], metabolism [59], and autophagy [60]. If a substantial portion of the p53 protein is sequestered in the cytoplasm, it logically follows that a lower concentration of p53 would be present in the nucleus. This reduced nuclear presence offers a plausible explanation for the impaired function observed for p53$_{N263Tfs*7}$, as it is unable to access its nuclear targets [61]. However p53$_{N263Tfs*7}$ does show some nuclear localisation, supporting the reduced activity [62]. This differential localisation thus provides a key mechanism underpinning the varied functional outcomes observed among different p53 mutants.

p53 exerts its tumour suppressive functions primarily as a transcription factor, binding to specific DNA REs

within the promoters of its target genes to regulate their expression [50, 63]. This leads to the induction of genes involved in cell cycle arrest, apoptosis, DNA repair, and senescence [64]. A common consequence of mutations in the p53 DBD is a loss of this critical transcriptional transactivation capability, thereby abrogating its tumour suppressor function [65, 66]. In the context of our study, luciferase reporter assays and qPCR provided clear evidence that $p53_{N263Tfs*7}$ exhibits significantly impaired transcriptional transactivation activity compared to $p53_{WT}$. Specifically, we observed a profound reduction in the ability of $p53_{N263Tfs*7}$ to activate *p21* and *BAX* transcription.

The observed deficiency in transcriptional activity for $p53_{N263Tfs*7}$ can be attributed to several mechanisms, many of which are interconnected. Foremost, its aberrant cytoplasmic sequestration would inherently limit the amount of protein able to reach the nucleus and interact with its DNA targets [61]. Beyond localisation defects, tetramerisation is often considered essential for the transcriptional activity of p53. Given that the $p53_{N263Tfs*7}$ does not possess a TD, the subsequent lack of tetramerisation is likely to impair the transcriptional activity of the p53 proteins that are localised to the nucleus [56]. The low-level of activity of $p53_{N263Tfs*7}$ observed in the reporter assays, may be driven by the ability of monomeric p53 units to bind their REs, albeit with a ~100-fold lower affinity compared to the functional homotetramer [67]. Importantly, this low level of activity, did not translate into significant induction of the endogenous p53 target genes *p21* or *BAX*. This apparent discrepancy may reflect the greater sensitivity of reporter assays, or suggest that the residual transcriptional activity of $p53_{N263Tfs*7}$ is insufficient to induce robust expression of endogenous target genes. Nevertheless, $p53_{N263Tfs*7}$ retained partial tumour suppressive activity in the proliferation, apoptosis and migration assays. It is therefore possible that these residual biological effects are mediated through low-level regulation of alternative p53 target genes that were not examined in this study and/or through transcription-independent functions of p53. Indeed, p53 has been shown to promote apoptosis directly at the mitochondria through interactions with BCL-2 family proteins, independently of its role as a transcription factor [68]. Given the predominantly cytoplasmic localisation of $p53_{N263Tfs*7}$, such mechanisms may contribute to the residual functional activity observed in our assays.

Co-transfection experiments further elucidated the functional characteristics of $p53_{N263Tfs*7}$. The behaviour of $p53_{N263Tfs*7}$ highlights an important distinction between truncating *TP53* variants and the more extensively studied missense mutations within the DNA-binding domain. Large-scale genotype-phenotype studies have shown that many missense mutants retain the ability to oligomerise with wild-type p53 and frequently exert dominant-negative effects that contribute substantially to pathogenicity [18, 19]. In contrast, truncating variants that remove the tetramerisation domain are predicted to be functionally distinct because they are unlikely to form heterotetramers with wild-type p53. Consistent with this model, co-transfection experiments demonstrated that $p53_{N263Tfs*7}$ did not inhibit the transcriptional activity of wild-type p53, indicating an absence of detectable dominant-negative activity. Rather than actively suppressing the remaining wild-type allele, $p53_{N263Tfs*7}$ appears to contribute to carcinogenesis through a quantitative reduction in functional p53 activity. The reduced transcriptional activity, impaired induction of p53 target genes, and diminished effects on proliferation, apoptosis and migration observed throughout this study support a hypomorphic loss-of-function phenotype. These findings add to growing evidence that *TP53* variants exist along a functional spectrum, ranging from dominant-negative and gain-of-function missense mutants to truncating alleles that retain limited residual tumour suppressor activity.

A limitation of this study is the use of HeLa and HEK293-derived cell lines for functional characterisation. Both cell types express viral proteins that are known to interact with the p53 pathway. In HeLa cells, the HPV E6 oncoprotein promotes p53 degradation [69], while adenoviral proteins expressed in HEK293 cells can modulate p53 stability and transcriptional responses [70]. These interactions may influence the magnitude of p53-dependent phenotypes observed in our assays. Nevertheless, all constructs were evaluated within the same cellular background, allowing direct comparison of relative differences between the p53 variants. Future studies using p53-null cellular models, would provide a cleaner genetic background in which to further define the intrinsic functional properties of $p53_{N263Tfs*7}$ and validate the observations reported here.

In summary, our comprehensive functional characterisation of the novel LFS associated $p53_{N263Tfs*7}$ mutant reveals a hypomorphic LOF phenotype, consistently demonstrated across localisation, transcriptional activity, cell growth, death and migration assays. We found that $p53_{N263Tfs*7}$ exhibits aberrant cytoplasmic sequestration due to the loss of key nuclear import/export signals, which significantly reduces its nuclear localisation. This mislocalisation, alongside the presumed structural inability to tetramerise, underpins the observed phenotype: a profound impairment of tumour suppressive functions, including transcriptional transactivation, and proliferative, apoptotic and migratory capacities. The absence of

DNE on $p53_{WT}$ suggests that $p53_{N263Tfs*7}$ behaves differently from many canonical DBD missense mutants, operating primarily as a hypomorphic LOF allele rather than an active inhibitor of wild-type p53. The distinct functional profile is consistent with a loss of tumour suppressor activity where the quantitative reduction in effective p53 is sufficient to drive disease. Specifically, the reduced nuclear concentration of functional p53 promotes aggressive cellular behaviour, contributing to increased proliferation and potential metastatic progression in the context of inherited cancer predisposition. Our findings demonstrate that oncogenesis in LFS can arise from partial impairments in p53 activity, rather than solely through dominant-negative or GOF mutations. Consequently, a more refined molecular classification of *TP53* variants that accounts for these hypomorphic LOF mutations could support more accurate predictions of cancer risk and disease progression in clinical practice.

Appendix A

Sequence information

Table 1 Forward and reverse primer sequences for site-directed mutagenesis of pTWIST-GFP-p53

Primer	Sequence
pTWIST-GFP-$p53_{C135Y}$ forward	5′-CCCTGCCCTCAACAAGATGTTTTACCAACTGGCCAA-3′
pTWIST-GFP-$p53_{C135Y}$ reverse	5′-TTGGCCAGTTGGTAAAACATCTTGTTGAGGGCAGGG-3′
pTWIST-GFP-$p53_{N263Tfs*7}$ forward	5′-ACTGGAAGACTCCAGTGGTACTGGGACGGAAC-3′
pTWIST-GFP-$p53_{N263Tfs*7}$ reverse	5′-GTTCCGTCCCAGTACCACTGGAGTCTTCCAGT-3′
pTWIST-GFP forward	5′-ATGGAGGAGCCGCAGTAAGATCCTAGCGTC-3′
pTWIST-GFP reverse	5′-GACGCTAGGATCTTACTGCGGCTCCTCCAT-3′

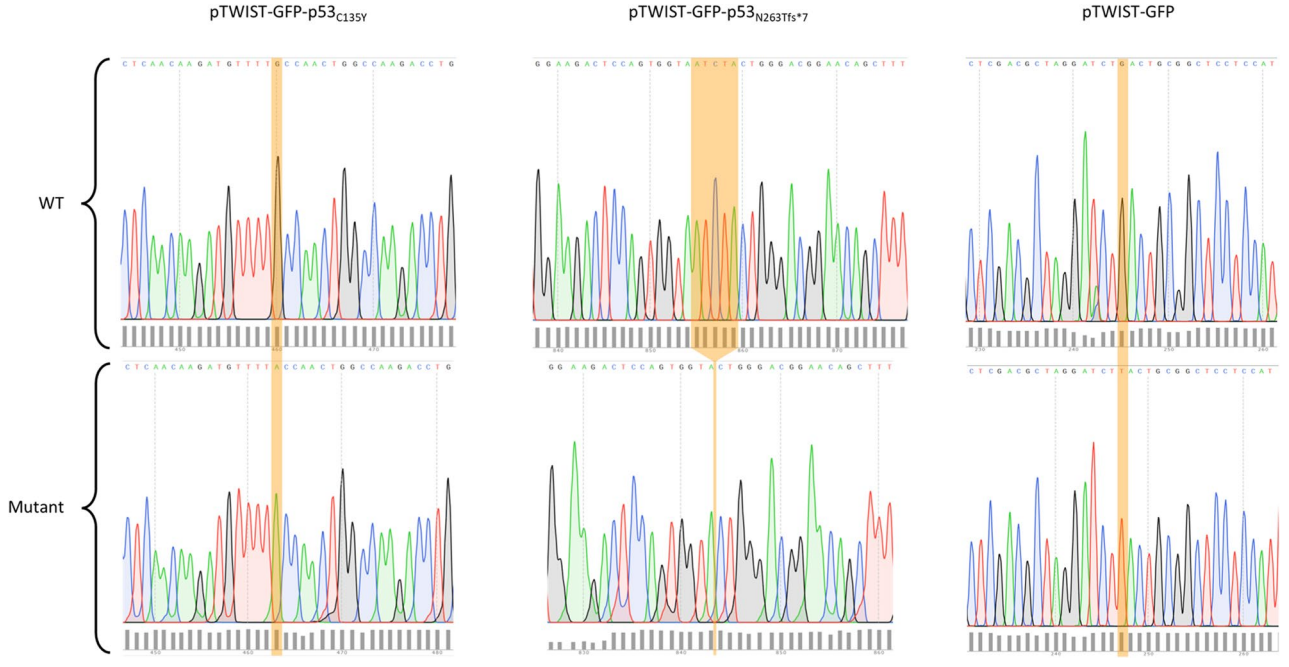


Fig. 8 Successful mutagenesis of pGFP-WT p53. Site-directed mutagenesis was performed using an Agilent QuikChange II Site-Directed Mutagenesis Kit, and successful mutagenesis was confirmed via sequencing. Chromatograms show successful the point mutations for pTWIST-GFP-$p53_{C135Y}$ and pTWIST-GFP, and the successful deletion for pTWIST-GFP-$p53_{p.N263Tfs*7}$

Table 2 Sequences for components of the CRISPR-Select^{TIME} assay

Component	Sequence
$p53_{N263Tfs*7}$ Donor DNA	5′-CCTCTTGCTTCTCTTTTCCTATCCTGAGTAGTGGTACTGGGACGGAACAGCTTTGAGGTGCGTGTTTGTG-3′
$p53_{SYN}$ Donor DNA	5′-TCTTGCTTCTCTTTTCCTATCCTGAGTAGTGGTAACCTACTGGGACGGAACAGCTTTGAGGTGCGTGTTTGT-3′
gRNA	5′-CCTGAGTAGTGGTAATCTAC-3′
PCR forward primer	5′-ACACTCTTTCCCTACACGACGCTCTTCCGATCTCCATACTACTACCCATCCACC-3′
PCR reverse primer	5′-GACTGGAGTTCAGACGTGTGCTCTTCCGATCTCTTGTCCTGCTTGCTTACC-3′

Table 3 MutScan Analysis of FASTQ Files. For each mutation, the left flanking sequence, specified mutation, and right flanking sequence were defined. MutScan was then used to identify the number of reads for each of the specified mutations

Left flanking sequence	Specified mutation	Right flanking sequence
N263Tfs*7		
CCTCTTGCTTCTCTTTTCCTATCCTGAGTAGTGGTA		CTGGGACGGAACAGCTTTGAGGTGCGTGTTTGTG
SYN		
CCTCTTGCTTCTCTTTTCCTATCCTGAGTAGTGGTAA	C	CTACTGGGACGGAACAGCTTTGAGGTGCGTGTTTGTG

Appendix B

Unprocessed western blots

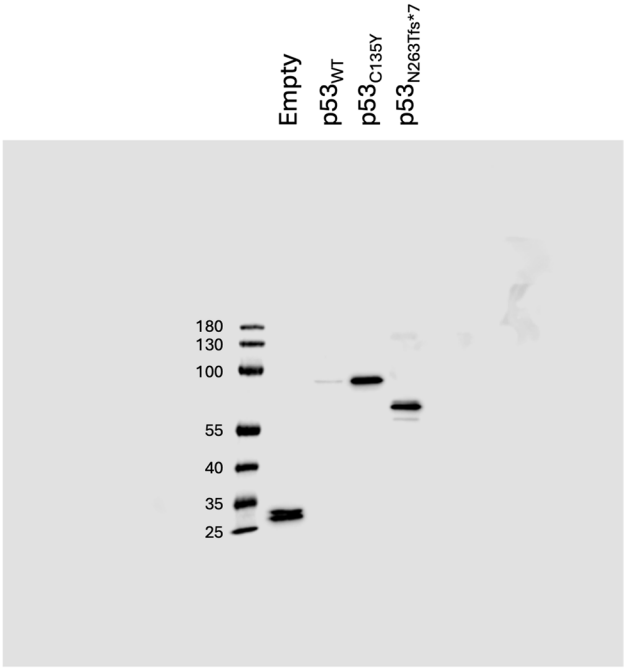


Fig. 9 Chemiluminescent detection of pTWIST-GFP-p53 constructs with anti-GFP. Unprocessed blots as presented in the manuscript Fig. 2

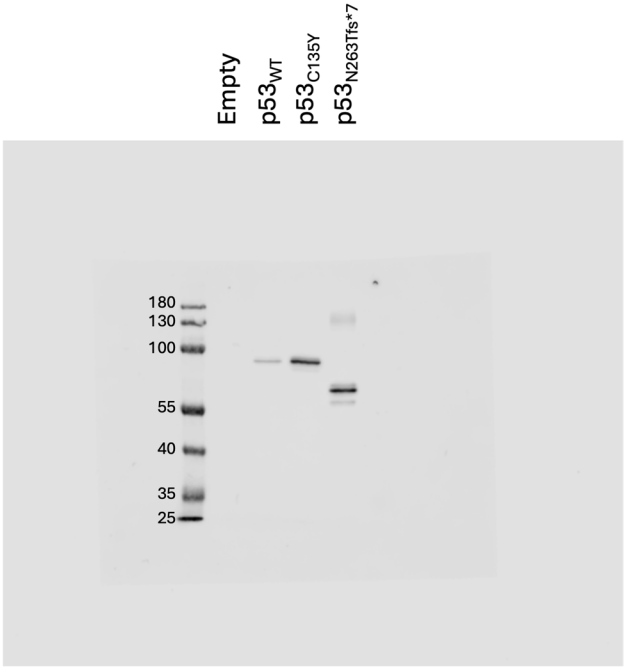


Fig. 10 Chemiluminescent detection of pTWIST-GFP-p53 constructs with anti-p53. Unprocessed blots as presented in the manuscript Fig. 2

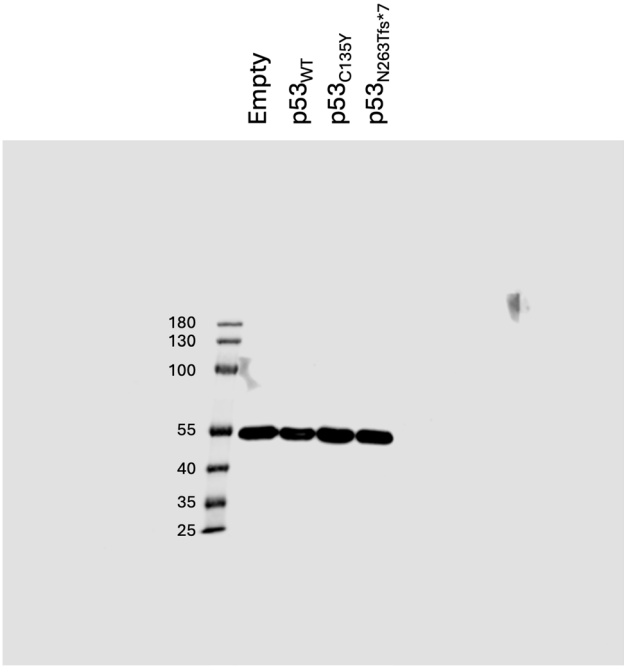


Fig. 11 Chemiluminescent detection of Tubulin. Unprocessed blots as presented in the manuscript Fig. 2

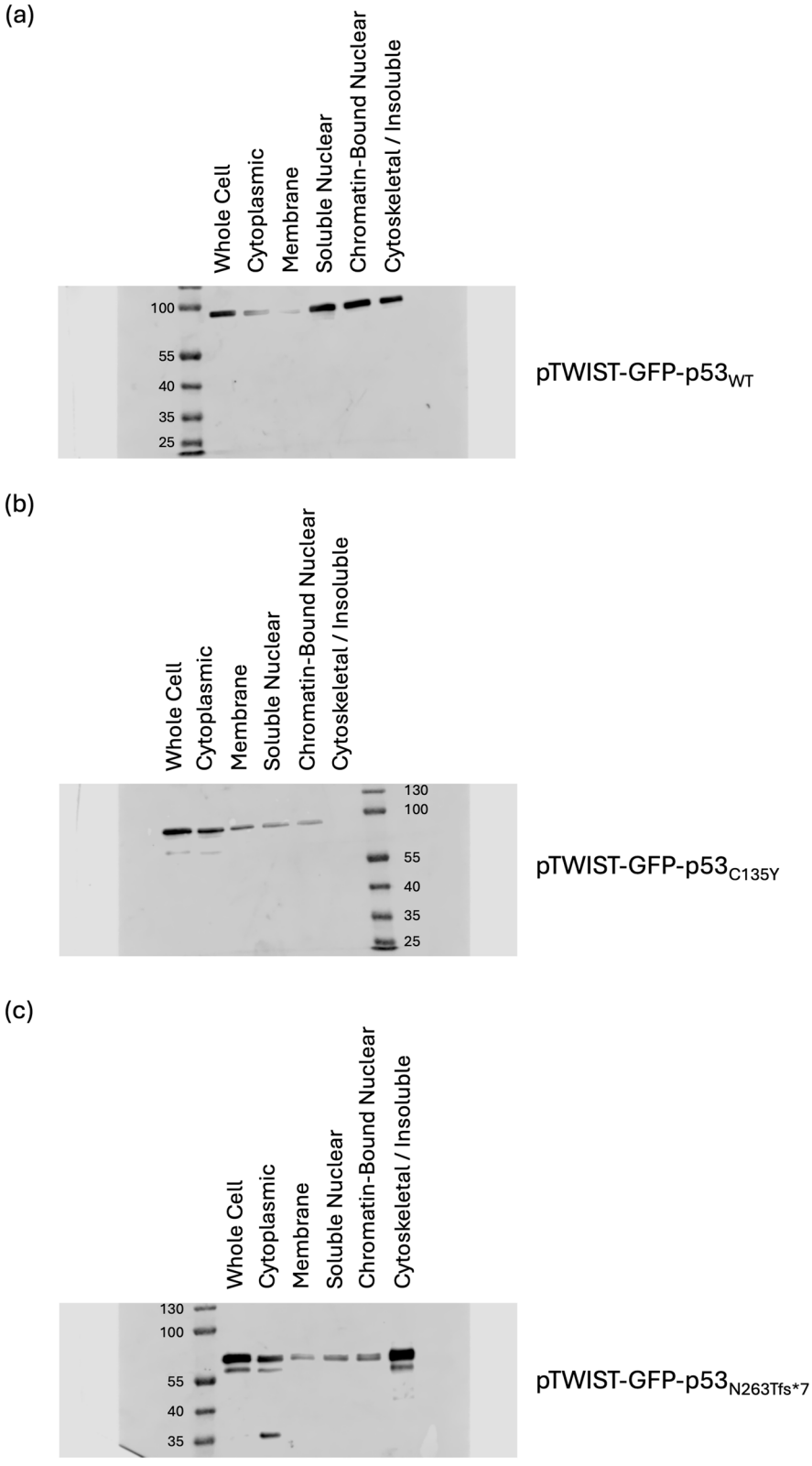


Fig. 12 Chemiluminescent detection of pTWIST-GFP-p53 constructs with anti-GFP after subcellular fractionation. Unprocessed blots for detection of **a** $p53_{WT}$, **b** $p53_{C135Y}$, and **c** $p53_{N263Tfs*7}$ as presented in the manuscript Fig. 3B

Abbreviations

DBD	DNA binding domain
DNE	Dominant-negative effects
GOF	Gain-of-function
LOF	Loss-of-function
NES	Nuclear export signal
NGS	Next generation sequencing
NLS	Nuclear localisation signal
REs	Response elements
SYN	Synonymous WT control
TD	Tetramerisation domain

Supplementary Information

The online version contains supplementary material available at https://doi.org/10.1186/s12885-026-16582-2.

Supplementary Material 1.

Acknowledgements

We would like to thank Dr Phil Reeves, members of the Genomics and Computational Biology research group at the University of Essex, and Lynwen James for their discussion and support.

Authors' contributions

FMW conducted the research, designed experiments, analysed data, and wrote the manuscript. MVM and GNB conceived the research, supervised experiments, designed the methods, analysed data, edited the manuscript. MVS, AY, and ZG provided samples, analysed data and contributed to critical analysis of the manuscript. AM and GW contributed to data analysis and manuscript editing.

Funding

This research was funded by the European Union-NextGenerationEU, through the National Recovery and Resilience Plan of the Republic of Bulgaria, project BG-RRP-2.004-0003.

Data availability

All data supporting the findings of this study are available within the paper and its Supplementary Information. Primer sequences and donor DNA sequences used in the CRISPR-Select experiments are provided in Supplementary Tables A1 and A2.

Declarations

Ethics approval and consent to participate

Not applicable.

Consent for publication

All authors agree to publish the manuscript.

Competing interests

The authors declare no competing interests.

Received: 9 March 2026 / Accepted: 16 July 2026
Published online: 29 July 2026

References

1. Li F, Fraumeni J. Soft-Tissue Sarcomas, Breast Cancer, and Other Neoplasms. Ann Intern Med. 1969;71(4):747–52. https://doi.org/10.7326/0003-4819-71-4-747.
2. Malkin D, Li FP, Strong LC, Fraumeni JF, Nelson CE, Kim DH, et al. Germ Line p53 Mutations in a Familial Syndrome of Breast Cancer, Sarcomas, and Other Neoplasms. Science. 1990;250(4985):1233–8. https://doi.org/10.1126/science.1978757.
3. Guha T, Malkin D. Inherited TP53 Mutations and the Li-Fraumeni Syndrome. Cold Spring Harb Perspect Med. 2017;7(4). https://doi.org/10.1101/cshperspect.a026187.
4. Kamihara J, Rana HQ, Garber JE. Germline TP53 Mutations and the Changing Landscape of Li-Fraumeni Syndrome. Hum Mutat. 2014;35(6):654–62. https://doi.org/10.1002/humu.22559.
5. Subasri V, Light N, Kanwar N, Brzezinski J, Luo P, Hansford JR, et al. Multiple Germline Events Contribute to Cancer Development in Patients with Li-Fraumeni Syndrome. Cancer Res Commun. 2023;3(5):738–54. https://doi.org/10.1158/2767-9764.Crc-22-0402.
6. Rizzotto D, Englmaier L, Villunger A. At a Crossroads to Cancer: How p53-Induced Cell Fate Decisions Secure Genome Integrity. Int J Mol Sci. 2021;22(19). https://doi.org/10.3390/ijms221910883.
7. Brooks CL, Gu W. Ubiquitination, phosphorylation and acetylation: the molecular basis for p53 regulation. Curr Opin Cell Biol. 2003;15(2):164–71. https://doi.org/10.1016/S0955-0674(03)00003-6.
8. Xu Y. Regulation of p53 responses by post-translational modifications. Cell Death Differ. 2003;10(4):400–3. https://doi.org/10.1038/sj.cdd.4401182.
9. Ouyang L, Shi Z, Zhao S, Wang FT, Zhou TT, Liu B, et al. Programmed cell death pathways in cancer: a review of apoptosis, autophagy and programmed necrosis. Cell Prolif. 2012;45(6):487–98. https://doi.org/10.1111/j.1365-2184.2012.00845.x.
10. Kato S, Han SY, Liu W, Otsuka K, Shibata H, Kanamaru R, et al. Understanding the function-structure and function-mutation relationships of p53 tumor suppressor protein by high-resolution missense mutation analysis. Proc Natl Acad Sci. 2003;100(14):8424–9. https://doi.org/10.1073/pnas.1431692100.
11. Wang H, Guo M, Wei H, Chen Y. Targeting p53 pathways: mechanisms, structures and advances in therapy. Signal Transduct Target Ther. 2023;8(1):92. https://doi.org/10.1038/s41392-023-01347-1.
12. Kennedy MC, Lowe SW. Mutant p53: it's not all one and the same. Cell Death Differ. 2022;29(5):983–7. https://doi.org/10.1038/s41418-022-00989-y.
13. Steele RJC, Thompson AM, Hall PA, Lane DP. The p53 tumour suppressor gene. BJS (Br J Surg). 1998;85(11):1460–7. https://doi.org/10.1046/j.1365-2168.1998.00910.x.
14. Alvarado-Ortiz E, de la Cruz-López KG, Becerril-Rico J, Sarabia-Sánchez MA, Ortiz-Sánchez E, García-Carrancá A. Mutant p53 Gain-of-Function: Role in Cancer Development, Progression, and Therapeutic Approaches. Front Cell Dev Biol. 2020;8:607670. https://doi.org/10.3389/fcell.2020.607670.
15. Willis A, Jung EJ, Wakefield T, Chen X. Mutant p53 exerts a dominant negative effect by preventing wild-type p53 from binding to the promoter of its target genes. Oncogene. 2004;23(13):2330–8. https://doi.org/10.1038/sj.onc.1207396.
16. Billant O, Léon A, Le Guellec S, Friocourt G, Blondel M, Voisset C. The dominant-negative interplay between p53, p63 and p73: A family affair. Oncotarget. 2016;7(43):69549–69564. https://doi.org/10.18632/oncotarget.11774.
17. Chan WM, Siu WY, Lau A, Poon RY. How many mutant p53 molecules are needed to inactivate a tetramer? Mol Cell Biol. 2004;24(8):3536–51. https://doi.org/10.1128/mcb.24.8.3536-3551.2004.
18. Bougeard G, Renaux-Petel M, Flaman JM, Charbonnier C, Fermey P, Belotti M, et al. Revisiting Li-Fraumeni Syndrome From TP53 Mutation Carriers. J Clin Oncol. 2015;33(21):2345–52. https://doi.org/10.1200/jco.2014.59.5728.
19. Giacomelli AO, Yang X, Lintner RE, McFarland JM, Duby M, Kim J, et al. Mutational processes shape the landscape of TP53 mutations in human cancer. Nat Genet. 2018;50(10):1381–7. https://doi.org/10.1038/s41588-018-0204-y.
20. Sorrell AD, Espenschied CR, Culver JO, Weitzel JN. Tumor protein p53 (TP53) testing and Li-Fraumeni syndrome: current status of clinical applications and future directions. Mol Diagn Ther. 2013;17(1):31–47. https://doi.org/10.1007/s40291-013-0020-0.
21. Sagne C, Marcel V, Bota M, Martel-Planche G, Nobrega A, Palmero EI, et al. Age at cancer onset in germline TP53 mutation carriers: association with polymorphisms in predicted G-quadruplex structures. Carcinogenesis. 2014;35(4):807–15. https://doi.org/10.1093/carcin/bgt381.
22. Schon K, Tischkowitz M. Clinical implications of germline mutations in breast cancer: TP53. Breast Cancer Res Treat. 2018;167(2):417–23. https://doi.org/10.1007/s10549-017-4531-y.
23. Chan CS. Prevalence and penetrance of Li-Fraumeni cancer predisposition syndrome. Curr Opin Syst Biol. 2017;1:48–53. https://doi.org/10.1016/j.coisb.2016.12.015.
24. Suzuki HI, Yamagata K, Sugimoto K, Iwamoto T, Kato S, Miyazono K. Modulation of microRNA processing by p53. Nature. 2009;460(7254):529–33. https://doi.org/10.1038/nature08199.
25. Brennan P. drawProteins: a Bioconductor/R package for reproducible and programmatic generation of protein schematics [version 1; peer review: 2 approved]. F1000Research. 2018;7(1105). https://doi.org/10.12688/f1000research.14541.1.
26. R Core Team. R: A Language and Environment for Statistical Computing. Vienna; 2025. https://www.R-project.org/.

27. Cerami E, Gao J, Dogrusoz U, Gross BE, Sumer SO, Aksoy BA, et al. The cBio cancer genomics portal: an open platform for exploring multidimensional cancer genomics data. Cancer Discov. 2012;2(5):401–4. https://doi.org/10.1158/2159-8290.Cd-12-0095.
28. Gao J, Aksoy BA, Dogrusoz U, Dresdner G, Gross B, Sumer SO, et al. Integrative analysis of complex cancer genomics and clinical profiles using the cBioPortal. Sci Signal. 2013;6(269):pl1. https://doi.org/10.1126/scisignal.2004088.
29. de Bruijn I, Kundra R, Mastrogiacomo B, Tran TN, Sikina L, Mazor T, et al. Analysis and Visualization of Longitudinal Genomic and Clinical Data from the AACR Project GENIE Biopharma Collaborative in cBioPortal. Cancer Res. 2023;83(23):3861–7. https://doi.org/10.1158/0008-5472.Can-23-0816.
30. Abramson J, Adler J, Dunger J, Evans R, Green T, Pritzel A, et al. Accurate structure prediction of biomolecular interactions with AlphaFold 3. Nature. 2024;630(8016):493–500. https://doi.org/10.1038/s41586-024-07487-w.
31. Chen Y, Zhang X, Dantas Machado AC, Ding Y, Chen Z, Qin PZ, et al. Structure of p53 binding to the BAX response element reveals DNA unwinding and compression to accommodate base-pair insertion. Nucleic Acids Res. 2013;41(17):8368–76. https://doi.org/10.1093/nar/gkt584.
32. Schrödinger, LLC. The PyMOL Molecular Graphics System, Version 1.8. 2015. https://www.schrodinger.com/
33. Brooke GN, Culley RL, Dart DA, Mann DJ, Gaughan L, McCracken SR, et al. FUS/TLS Is a Novel Mediator of Androgen-Dependent Cell-Cycle Progression and Prostate Cancer Growth. Can Res. 2011;71(3):914–24. https://doi.org/10.1158/0008-5472.Can-10-0874.
34. Schneider CA, Rasband WS, Eliceiri KW. NIH Image to ImageJ: 25 years of image analysis. Nat Methods. 2012;9(7):671–5. https://doi.org/10.1038/nmeth.2089.
35. Chen C, Okayama H. High-Efficiency Transformation of Mammalian Cells by Plasmid DNA. Mol Cell Biol. 1987;7(8):2745–52. https://doi.org/10.1128/mcb.7.8.2745-2752.1987.
36. Brooke GN, Parker MG, Bevan CL. Mechanisms of androgen receptor activation in advanced prostate cancer: differential co-activator recruitment and gene expression. Oncogene. 2008;27(21):2941–50. https://doi.org/10.1038/sj.onc.1210955.
37. Leach DA, Mohr A, Giotis ES, Cil E, Isac AM, Yates LL, et al. The antiandrogen enzalutamide downregulates TMPRSS2 and reduces cellular entry of SARS-CoV-2 in human lung cells. Nat Commun. 2021;12(1):4068. https://doi.org/10.1038/s41467-021-24342-y.
38. Suarez-Arnedo A, Torres Figueroa F, Clavijo C, Arbeláez P, Cruz JC, Muñoz-Camargo C. An image J plugin for the high throughput image analysis of in vitro scratch wound healing assays. PLoS ONE. 2020;15(7):e0232565. https://doi.org/10.1371/journal.pone.0232565.
39. Thermo Fisher Scientific. Invitrogen TrueDesign Genome Editor. 2023. https://www.thermofisher.com/uk/en/home/life-science/genome-editing/invitrogen-truedesign-genome-editor.html. Accessed 4 May 2023.
40. Chen S, Huang T, Wen T, Li H, Xu M, Gu J. MutScan: fast detection and visualization of target mutations by scanning FASTQ data. BMC Bioinformatics. 2018;19(1):16. https://doi.org/10.1186/s12859-018-2024-6.
41. Ashcroft M, Vousden KH. Regulation of p53 stability. Oncogene. 1999;18(53):7637–43. https://doi.org/10.1038/sj.onc.1203012.
42. Niu Y, Ferreira Azevedo CA, Li X, Kamali E, Haagen Nielsen O, Storgaard Sørensen C, et al. Multiparametric and accurate functional analysis of genetic sequence variants using CRISPR-Select. Nat Genet. 2022;54(12):1983–93. https://doi.org/10.1038/s41588-022-01224-7.
43. Muller PA, Vousden KH, Norman JC. p53 and its mutants in tumor cell migration and invasion. J Cell Biol. 2011;192(2):209–18. https://doi.org/10.1083/jcb.201009059.
44. Chen X, Zhang T, Su W, Dou Z, Zhao D, Jin X, et al. Mutant p53 in cancer: from molecular mechanism to therapeutic modulation. Cell Death Dis. 2022;13(11):974. https://doi.org/10.1038/s41419-022-05408-1.
45. Ethayathulla AS, Nguyen HT, Viadiu H. Crystal Structures of the DNA-binding Domain Tetramer of the p53 Tumor Suppressor Family Member p73 Bound to Different Full-site Response Elements. J Biol Chem. 2013;288(7):4744–54. https://doi.org/10.1074/jbc.M112.408039.
46. Ho WC, Fitzgerald MX, Marmorstein R. Structure of the p53 Core Domain Dimer Bound to DNA. J Biol Chem. 2006;281(29):20494–502. https://doi.org/10.1074/jbc.M603634200.
47. Golovenko D, Bräuning B, Vyas P, Haran TE, Rozenberg H, Shakked Z. New Insights into the Role of DNA Shape on Its Recognition by p53 Proteins. Structure. 2018;26(9):1237-1250.e6. https://doi.org/10.1016/j.str.2018.06.006.
48. Garg A, Hazra JP, Sannigrahi MK, Rakshit S, Sinha S. Variable Mutations at the p53–R273 Oncogenic Hotspot Position Leads to Altered Properties. Biophys J. 2020;118(3):720–8. https://doi.org/10.1016/j.bpj.2019.12.015.
49. Olivier M, Hollstein M, Hainaut P. TP53 mutations in human cancers: origins, consequences, and clinical use. Cold Spring Harb Perspect Biol. 2010;2(1):a001008. https://doi.org/10.1101/cshperspect.a001008.
50. Hernández Borrero LJ, El-Deiry WS. Tumor suppressor p53: Biology, signaling pathways, and therapeutic targeting. Biochim Biophys Acta Rev Cancer. 2021;1876(1):188556. https://doi.org/10.1016/j.bbcan.2021.188556.
51. Nie L, Sasaki M, Maki CG. Regulation of p53 Nuclear Export through Sequential Changes in Conformation and Ubiquitination *. J Biol Chem. 2007;282(19):14616–25. https://doi.org/10.1074/jbc.M610515200.
52. Iwahashi N, Ikezaki M, Komohara Y, Fujiwara Y, Noguchi T, Nishioka K. Cytoplasmic p53 aggregates accumulated in p53-mutated cancer correlate with poor prognosis. PNAS Nexus. 2022;1(3). https://doi.org/10.1093/pnasnexus/pgac128.
53. Nishitsuji K, Mito R, Ikezaki M, Yano H, Fujiwara Y, Matsubara E, et al. Impacts of cytoplasmic p53 aggregates on the prognosis and the transcriptome in lung squamous cell carcinoma. Cancer Sci. 2024;115(9):2947–60. https://doi.org/10.1111/cas.16252.
54. Harris CC. Structure and Function of the p53 Tumor Suppressor Gene: Clues for Rational Cancer Therapeutic Strategies. JNCI J Natl Cancer Inst. 1996;88(20):1442–55. https://doi.org/10.1093/jnci/88.20.1442.
55. Liang SH, Clarke MF. A Bipartite Nuclear Localization Signal Is Required for p53 Nuclear Import Regulated by a Carboxyl-terminal Domain*. J Biol Chem. 1999;274(46):32699–703. https://doi.org/10.1074/jbc.274.46.32699.
56. Itahana Y, Ke H, Zhang Y. p53 Oligomerization Is Essential for Its C-terminal Lysine Acetylation*. J Biol Chem. 2009;284(8):5158–64. https://doi.org/10.1074/jbc.M805696200.
57. Klotzsche O, Etzrodt D, Hohenberg H, Bohn W, Deppert W. Cytoplasmic retention of mutant tsp53 is dependent on an intermediate filament protein (Vimentin) scaffold. Oncogene. 1998;16(26):3423–34. https://doi.org/10.1038/sj.onc.1202155.
58. Baptiste N, Prives C. p53 in the Cytoplasm: A Question of Overkill? Cell. 2004;116(4):487–9. https://doi.org/10.1016/S0092-8674(04)00164-3.
59. Sanford JD, Jin A, Grois GA, Zhang Y. A role of cytoplasmic p53 in the regulation of metabolism shown by bat-mimicking p53 NLS mutant mice. Cell Rep. 2023;42(1):111920. https://doi.org/10.1016/j.celrep.2022.111920.
60. Green DR, Kroemer G. Cytoplasmic functions of the tumour suppressor p53. Nature. 2009;458(7242):1127–30. https://doi.org/10.1038/nature07986.
61. Kastan MB, Zambetti GP. Parc-ing p53 in the Cytoplasm. Cell. 2003;112(1):1–2. https://doi.org/10.1016/S0092-8674(02)01281-3.
62. Giannakakou P, Sackett DL, Ward Y, Webster KR, Blagosklonny MV, Fojo T. p53 is associated with cellular microtubules and is transported to the nucleus by dynein. Nat Cell Biol. 2000;2(10):709–17. https://doi.org/10.1038/35036335.
63. Fischer M. Census and evaluation of p53 target genes. Oncogene. 2017;36(28):3943–3956. 1476-5594 Fischer, M Orcid: 0000-0002-3429-1876 Journal Article Research Support, Non-U.S. Gov't Review England 2017/03/14 Oncogene. 2017;36(28):3943-3956. Epub 2017 Mar 13. https://doi.org/10.1038/onc.2016.502.
64. Mijit M, Caracciolo V, Melillo A, Amicarelli F, Giordano A. Role of p53 in the Regulation of Cellular Senescence. Biomolecules. 2020;10(3). https://doi.org/10.3390/biom10030420.
65. Raycroft L, Wu H, Lozano G. Transcriptional Activation by Wild-Type but Not Transforming Mutants of the p53 Anti-Oncogene. Science. 1990;249(4972):1049–51. https://doi.org/10.1126/science.2144364.
66. Vikhanskaya F, Lee MK, Mazzoletti M, Broggini M, Sabapathy K. Cancer-derived p53 mutants suppress p53-target gene expression–potential mechanism for gain of function of mutant p53. Nucleic Acids Res. 2007;35(6):2093–104. https://doi.org/10.1093/nar/gkm099.
67. Kamada R, Toguchi Y, Nomura T, Imagawa T, Sakaguchi K. Tetramer formation of tumor suppressor protein p53: Structure, function, and applications. Pept Sci. 2016;106(4):598–612. https://doi.org/10.1002/bip.22772.
68. Mihara M, Erster S, Zaika A, Petrenko O, Chittenden T, Pancoska P, et al. p53 has a direct apoptogenic role at the mitochondria. Mol Cell. 2003;11(3):577–90. https://doi.org/10.1016/s1097-2765(03)00050-9.
69. Yi JW, Jang M, Kim SJ, Kim SS, Rhee JE. Degradation of p53 by natural variants of the E6 protein of human papillomavirus type 16. Oncol Rep. 2013;29(4):1617–22. https://doi.org/10.3892/or.2013.2281.
70. Muller S, Dobner T. The adenovirus E1B–55K oncoprotein induces SUMO modification of p53. Cell Cycle. 2008;7(6):754–8. https://doi.org/10.4161/cc.7.6.5495.

Publisher's Note

Springer Nature remains neutral with regard to jurisdictional claims in published maps and institutional affiliations.